Hindawi
Discrete Dynamics in Nature and Society
Volume 2018, Article ID 3498057, 13 pages
https://doi.org/10.1155/2018/3498057

Research Article

Nonsmooth Vibration Characteristic of Gear Pair System with Periodic Stiffness and Backlash

Minjia He,[1,2] Shuo Li,[2] Zhenjun Lin,[2] Jinjin Wang,[1,2] Shuang Liu,[1,2] and Ruolan Hao[2]

[1]*Liren College of Yanshan University, Qinhuangdao, China*
[2]*College of Electrical Engineering, Yanshan University, Qinhuangdao, China*

Correspondence should be addressed to Shuang Liu; shliu@ysu.edu.cn

Received 8 March 2018; Accepted 24 May 2018; Published 8 July 2018

Academic Editor: Jorge E. Macias-Diaz

As the most widely used power transmission device in mechanical equipment, the vibration characteristics of gears have a very important influence on the working performance. It is of great theoretical and practical significance to study the vibration characteristics of gear system. In this paper, a gear transmission system model is set up in a forcefully nonlinear form; the continuity mapping and discontinuity mapping are utilized to analyze the nonsmooth vibration. Then, the sliding dynamics of separation boundaries is studied by using the perturbation method and the differential inclusion theory. In addition, the periodic response of gear pair system is illustrated and Floquet's theory is presented to confirm the stability and bifurcation of periodic response. Concurrently, the maximal Lyapunov exponent is obtained to accurately determine the chaotic state in gear pair system, which is consistent with the bifurcation diagram and Poincare section. Finally, a reasonable explanation is given for the jump phenomenon in bifurcation diagram.

1. Introduction

The gear system is widely used in various mechanical systems and equipment because of its compact structure and high transmission efficiency. Its own vibration characteristics can directly affect the performance and reliability of the whole system. Therefore, the study of its vibration characteristics has great significance.

Dating back to 1980s, many researchers had carried out experiments on the nonlinear vibration of gear system [1–5]; besides a certain number of complicated phenomena such as bifurcation and chaos had been observed. In [6], the nonlinear frequency response characteristics of a gear transmission system with backlash had been studied by the harmonic balance method. In [7], some experiments had been carried out on a gear pair transmission system. In addition several phenomena such as chaotic behaviors of subharmonic resonance and superharmonic resonance had been studied. In [8], a nonlinear rotor-bearing system was observed; bifurcations and the periodic responses were also investigated. Moreover, the chaotic response was checked as well through using the Lyapunov exponent and numerical methods. In [9], a research on a nonlinear model of gear transmission system including backlash, friction, and time-varying stiffness was achieved. On the contrary, the existence of bifurcation, periodic responses, and chaotic motions were studied numerically. In [10], the frequency responses of a nonlinear geared rotor-bearing system with time-varying mesh stiffness were inspected by the methods of multiple-scales and mathematical simulation. In [11], the vibration dynamic responses of a gear transmission system supported by journal bearing were studied; besides the subharmonic, periodic, and chaotic states were examined.

What is more, plenty of valuable research had been commenced on gear transmission system. But they rarely involved the nonsmooth dynamics of gear system. More precisely, the gear transmission system is a typical system with segmented properties, caused by the presence of backlash. Moreover, with the presence of backlash, the gear transmission system can be considered as one of vibration shock systems. At the beginning of this century, considerable researchers were interested in this system, especially in segmented linear systems that were stimulated by external periodic forces. In [12], the earliest research for a segmented linear system without

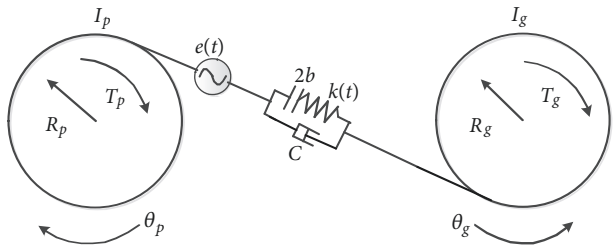

Figure 1: The gear transmission model.

damping was made and a closed solution of the periodic response was obtained. In [13], a mapping technique was developed to investigate a discrete linear system; besides the chaotic behavior was presented in numerical representation. In [14], a mapping approach was adopted to observe the periodic response and bifurcation of a segmented linear oscillator. In [15], a mapping structure for discontinuous system was initially proposed; the idea of mapping structure was used to investigate a periodic segmented linear system. In addition, the investigations can serve as examples in [16–18].

In all those works, a continuous mapping method was applied to transform nonsmooth gear system into segmented linear system, which can not explain the nonsmooth dynamic behavior of gear system completely. A large number of common problems can be described by discrete dynamic systems even if the problems are described by continuous dynamic systems. In this paper, the Poincare section and bifurcation diagram are obtained by numerical simulation, and the dynamic performance of gear transmission system is studied. In this paper, we construct discontinuous mapping, and combining with Floquet theory, we study the local dynamic characteristics of clearance and its front and rear, which reveal the vibration mechanism of gear transmission system in the gap nonsmooth state. The organization of this paper is as follows. Firstly, this paper briefly introduces a gear drive model with the basic dynamic response of a typical gear drive system. Then, the continuity mapping and discontinuity mapping are set up systematically. What is more, the differential inclusion theory and the method of perturbation are adopted to investigate the singularity of the sliding dynamics on separation boundaries, and the periodic response is analyzed by the mapping method. In addition, the discretization is a very important tool for analyzing the stability of the periodic motion in the gear system. The discrete-time shooting method is adopted to calculate the change of the Floquet multiplier. Then, the Floquet theory and the idea of mapping are introduced to give the methods and conditions for judging the periodic response of the system. At last, a summary of this work is presented.

2. The Mechanical Model

When both the bearing support of the entire system and the stiffness of the drive shaft are large for the gears in the transmission system, the torsional vibration model can be simplified as the form shown in Figure 1.

If the vibration between teeth is ignored in the gear system, the time-varying stiffness and static transmission error of the basic oscillation frequency are equal to the gear meshing frequency:

$$\omega_h = n_p\omega_p = n_g\omega_g \tag{1}$$

n_p and n_g represent the number of teeth in the driving wheel and the driven wheel, respectively. This means that the time-varying stiffness and static transmission error of the system can be expressed in a form of Fourier to Fourier series:

$$k(t) = k_0 + \sum_{m=1}^{\infty} k_m \cos\left(m\omega_h t + \varphi_m t\right) \tag{2}$$

Through Newton's theorem, the balance equation of driving wheel and driven wheel can be written as

$$\begin{aligned} &I_P\ddot{\theta}_P + CR_P\left[R_P\dot{\theta}_P - R_g\dot{\theta}_g - \dot{e}(t)\right] \\ &\quad + K(t)R_P f\left[R_P\theta_P - R_g\theta_g - e(t)\right] = T_P \end{aligned} \tag{3}$$

$$\begin{aligned} &I_g\ddot{\theta}_g - CR_g\left[R_P\ddot{\theta}_P - R_g\dot{\theta}_g - \dot{e}(t)\right] \\ &\quad - K(t)R_g f\left[R_P\theta_P - R_g\theta_g - e(t)\right] = -T_g \end{aligned} \tag{4}$$

I_p and I_g are, respectively, the rotational inertia of the driving gear and the driven gear, θ_p and θ_g are, respectively, the angular displacement of driving gear and driven gear, R_p and R_g are, respectively, the radius of base circle of driving gear and the driven gear, and T_p and T_g are, respectively, the load torque of driving wheel and wheel. In addition, $k(t)$ is the time-varying meshing stiffness, $e(t)$ is the transmission error, and c is the mesh damping.

By assuming that $x = R_P\theta_P - R_g\theta_g - e(t)$, (3) and (4) can be transformed as

$$m_e\ddot{x} + c\dot{x} + k(t)f(x) = F_{av} + F_e \tag{5}$$

$m_e = I_pI_g/(I_gR_P^2 + I_pR_g^2)$; $F_e = -m_e\ddot{e}(t)$; $F_{av} = m_e * (R_pT_p/I_p + R_gT_g/I_g)$.

Because the time-varying stiffness and static transmission error of the basic oscillation frequency are equal to the gear meshing frequency ω_h, the mesh stiffness and the static transmission error terms can be expressed in the form of Fourier series. Taking the first harmonic,

$$\begin{aligned} k(t) &= k_0 + k_1\cos\left(\omega_h t\right), \\ e(t) &= e_m\cos\left(\omega_h t + \varphi_e\right) \end{aligned} \tag{6}$$

k_0 is the average stiffness, and k_1 is the fluctuation amplitude. Assuming that $\tau = \omega_0 t$, $\omega_0 = \sqrt{k_0/m_e}$, $\xi = c/2\sqrt{m_e k_0}$, $k(\tau) = k(t)/k_0$, $\omega = \omega_h/\omega_0$, $u(\tau) = x(t)/b$, and replacing τ with t, then the dynamic model can be simplified as follows:

$$\begin{aligned} \ddot{u} + 2\xi\dot{u} + k(t)f(u) &= f_{av} + f_e\omega^2\cos\left(\omega t + \varphi\right), \\ e(t) &= e_m\cos\left(\omega_h t + \varphi_e\right) \end{aligned} \tag{7}$$

And $f_{av} = F_{av}/bk_0$, $f_e = e_m/b$, $k(t) = 1 + k_1 \cos(\omega t)$,

$$f(u) = \begin{cases} u - 1 & u \geq 1 \\ 0 & -1 \leq u \leq 1 \\ u + 1 & u \leq -1 \end{cases} \tag{8}$$

From (7), the mechanical model is set up. Because the gear system is a typical nonsmooth system, the previous method about smooth is not applicable. Therefore, a mapping method is utilized to analyze the nonsmooth system.

3. The Construction of Mapping

For the gear model in this paper, due to the backlash, time-varying stiffness, and static transmission error, a variety of complex motion patterns may occur between the driving wheel and the driven wheel, so it is necessary to establish different mappings to study each movement. There are three main cases and corresponding mapping methods.

(1) The Meshing State. In this case, the system flow does not pass through the constraint surface. But in a smooth area, the operating state of the system is continuous and smooth, and it can be analyzed by continuous smooth theory.

(2) The Collision State. In this case, the system flow moves from one subinterval through the constraint surface to another subinterval. The Jacobi matrix of the system has a jump when the flow crosses over the constraint surface. A discontinuous mapping is necessary to compensate for the system flow jump, and then the composite mapping method can be used to analyze the whole system.

(3) The Edge State. In this case, the teeth of driving wheel are in contact with the teeth of driven wheel at a relative zero speed, which is a critical situation. The system flow is tangent to a constraint in a subinterval. Edge theory can be used to study this condition; besides the discontinuous mapping is used to analyze the local characteristics.

3.1. The Basic Mapping. For the gear pair system (7), the phase space is divided into three subdomains by two separation boundaries and the corresponding phase space is defined as

$$\begin{aligned} D_1 &= \{(u, \dot{u}) \mid u \in (1, \infty), \dot{u} \in (-\infty, +\infty)\} \\ D_2 &= \{(u, \dot{u}) \mid u \in (-1, 1), \dot{u} \in (-\infty, +\infty)\} \\ D_3 &= \{(u, \dot{u}) \mid u \in (-\infty, -1), \dot{u} \in (-\infty, +\infty)\} \end{aligned} \tag{9}$$

The two constraint surfaces are defined as

$$\begin{aligned} D_{12} &= \{(u, \dot{u}) \mid u = 1, \dot{u} \in (-\infty, +\infty)\} \\ D_{23} &= \{(u, \dot{u}) \mid u = -1, \dot{u} \in (-\infty, +\infty)\} \end{aligned} \tag{10}$$

In order to establish the mapping, the two constraints can be further divided, $D_{12} = \partial D_{12} \cup \partial D_{21} \cup (1, 0)$, $D_{23} = \partial D_{23} \cup \partial D_{32} \cup (-1, 0)$, and the four subsets are defined as

$$\begin{aligned} \partial D_{12} &= \{(u, \dot{u}) \mid u = 1, \dot{u} < 0\} \\ \partial D_{21} &= \{(u, \dot{u}) \mid u = 1, \dot{u} > 0\} \\ \partial D_{23} &= \{(u, \dot{u}) \mid u = -1, \dot{u} < 0\} \\ \partial D_{32} &= \{(u, \dot{u}) \mid u = -1, \dot{u} > 0\} \end{aligned} \tag{11}$$

From the four subsets, all the six basic mappings are defined as shown in Figure 2.

$$\begin{aligned} &P_1\colon \partial D_{21} \longrightarrow \partial D_{12}, \\ &P_2\colon \partial D_{21} \longrightarrow \partial D_{23}, \\ &P_3\colon \partial D_{23} \longrightarrow \partial D_{32}, \\ &P_4\colon \partial D_{32} \longrightarrow \partial D_{21}, \\ &P_5\colon \partial D_{12} \longrightarrow \partial D_{21}, \\ &P_6\colon \partial D_{32} \longrightarrow \partial D_{23} \end{aligned} \tag{12}$$

3.2. Discontinuous Mapping. Discontinuous mapping is a conversion relationship that represents the flow of the system between two adjacent subintervals. This transformation is to compensate for the discontinuity of the system flow at the constraint surface. Considering the gear pair system in this paper, it is used to compensate for the discontinuity of the teeth during the transition between the disengaged state and the meshing state. The motion between the driving wheel teeth and the driven wheel teeth mainly includes three cases; the relationship between the system flow and the constraint surface is different from the cases (2) and (3), which are the collision state and the edge state. Therefore, it is necessary to introduce two types of discontinuous mappings, which are noncritical discontinuous mapping and critical discontinuous mapping.

The noncritical discontinuous mapping is to compensate for the discontinuity of the system's flow through the constraint surface. The figure is shown in Figure 3.

t_p is the time that the undamaged line $x(t)$ reaches the interface S; $\bar{t}$ is the time that the disturbed trajectory reaches the constraint surface S; $\delta x_0 = \tilde{x}_0 - x_0$ is the initial disturbance value; $\delta x_{p-} = \tilde{x}(\bar{t}_p) - x(\bar{t}_p)$ represents the disturbance value in the subspace before crossing the boundary D_-; $\delta x_{p+} = \tilde{x}(\bar{t}_p) - x(\bar{t}_p)$ is the disturbance value in the subspace after crossing the boundary D_-. Assuming that $\delta x_{p+} = S_{21}\delta x_{p-}$, S_{21} represents the transition from the subspace D_- across the

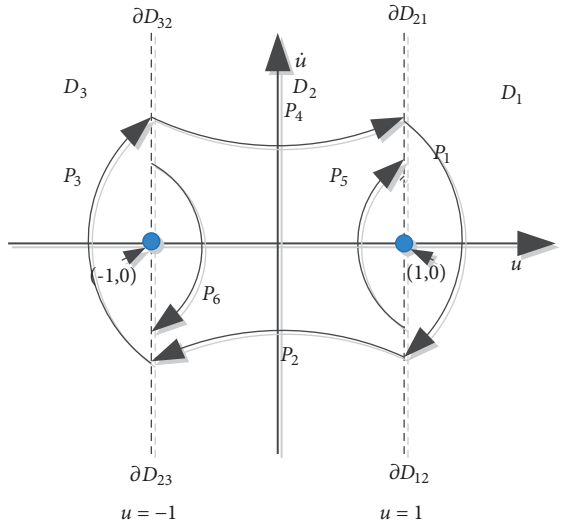

Figure 2: The basic mapping.

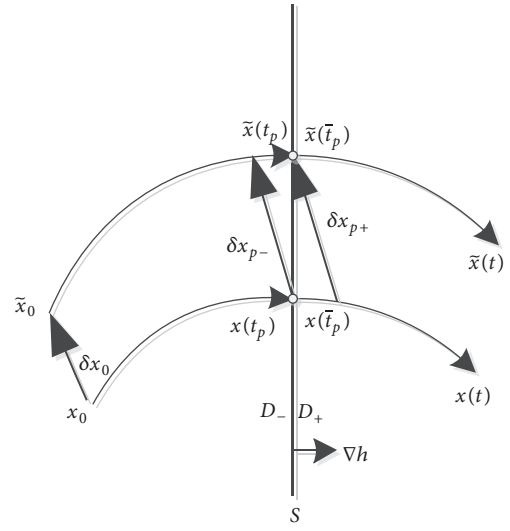

Figure 3: The noncritical discontinuous mapping.

interface to the subspace D_+. Make the trajectory δx_{p+} in front of t_p the first-order Taylor expansion.

$$\begin{aligned}\delta x_{p+} &= \tilde{x}\left(\bar{t}_p\right) - x\left(\bar{t}_p\right)\\ &\approx \left(\tilde{x}\left(t_p\right) + f_{p-}\delta t\right) - \left(x\left(t_p\right) + f_{p+}\delta t\right)\\ &\approx \left(\tilde{x}\left(t_p\right) - x\left(t_p\right)\right) + \left(f_{p-}\delta t - f_{p+}\delta t\right)\\ &\approx \delta x_{p-} + \left(f_{p-} - f_{p+}\right)\delta t\end{aligned} \tag{13}$$

$\delta t = \bar{t}_p - t_p$ is the time which $\tilde{x}(t)$ reaches the constraint surface after the trajectory $x(t)$ reaches the interface. According to the analysis of the transition point conditions $h(x) = 0$,

$$\delta t = -\frac{\nabla h \delta x_{p-}}{\nabla h f_{p-}} \tag{14}$$

From (13) and (14),

$$\begin{aligned}\delta x_{p+} &= \delta x_{p-} + \left(f_{p-} - f_{p+}\right)\delta t\\ &= \delta x_{p-} + \left(f_{p-} - f_{p+}\right)\left(-\frac{\nabla h \delta x_{p-}}{\nabla h f_{p-}}\right)\\ &= \left(I + \frac{\left(f_{p+} - f_{p-}\right)\nabla h}{\nabla h f_{p-}}\right)\delta x_{p-}\end{aligned} \tag{15}$$

Then

$$S_{21} = I + \frac{\left(f_{p+} - f_{p-}\right)\nabla h}{\nabla h f_{p-}} \tag{16}$$

If it is reversible, then

$$S_{21} = I + \frac{\left(f_{p+} - f_{p-}\right)\nabla h}{\nabla h f_{p-}} \tag{17}$$

Equations (16) and (17) are the noncritical discontinuous mapping. When the state of motion of the gear system transitions between teeth and meshing happens, it is necessary to introduce the above discontinuous mapping.

The critical discontinuous mapping is to compensate for discontinuities when the system flow near the edge of the wipe traverses the interface.

The discontinuous mapping of the critical situation is the discontinuous mapping when the edge is bifurcated. For the vector field segmented smooth system, the vector field is given as follows:

$$\dot{X} = \begin{cases} F_1(x), & H(x) < 0\\ F_2(x), & H(x) > 0\end{cases} \tag{18}$$

$$X \in R^n,\ F_i : R^n \longmapsto R^n,\ H : R^n \longmapsto R$$

$i = 1, 2$. Define the switching plane or interface as follows: $\sum = \{x \in R^n \mid H(x) = 0\}$. The switching surface corresponds to the constraint surface of the model. The interface divides the phase space of the system into two parts, $S^- = \{x \in R^n \mid H(x) < 0\}$, $S^+ = \{x \in R^n \mid H(x) > 0\}$. Assuming that, in S^-, the motion is determined by the flow $\Phi_1(t)$; in S^+, the motion is determined by the flow $\Phi_2(t)$. The phase space is shown in Figure 4.

If bifurcation occurs in the system at the edge of (x^*, t^*), it should meet the analytical conditions:

$$\begin{aligned}&H\left(x^*\right) = 0,\\ &\nabla H\left(x^*\right) \neq 0\\ &\left\langle \nabla H\left(x^*\right), \frac{\partial \phi_i}{\partial t}\left(x^*, t^*\right)\right\rangle = \left\langle \nabla H, F_i\right\rangle = 0\\ &\frac{d^2}{dt^2} H\left(\phi_i\left(x^*, t^*\right)\right)\Big|_{X=X^*, t=t^*}\\ &= \left\langle \nabla H, \frac{\partial H}{\partial x} F_i\right\rangle + \left\langle \frac{\partial^2 H}{\partial x^2} F_i, F_i\right\rangle > 0\end{aligned} \tag{19}$$

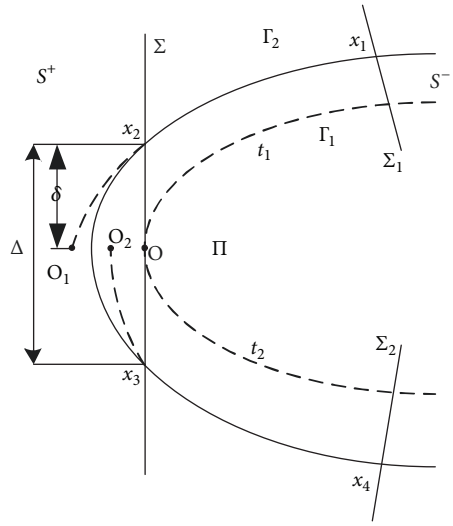

Figure 4: The critical discontinuous mapping.

In general, the bifurcation point can be converted to by coordinate transformation. In this paper, the analytical form of the discontinuity map is ignored. We just give the conclusion that the local mapping in the neighborhood of grazing point has a 3/2-type singularity.

3.3. Local Singularity. The sliding dynamics along the separation boundaries will be investigated in this section by using the perturbation method and the differential inclusion theory.

For (7), suppose $x_1 = u$, $x_2 = \dot{u}$, then

$$\begin{aligned}\dot{x}_1 &= x_2\\ \dot{x}_2 &= -2\xi x_2 - \left(1 + k_1\cos(\omega t)\right) * f\left(x_1\right) + f_{av}\\ &\quad + f_e\omega^2\cos(\omega t)\end{aligned} \tag{20}$$

where

$$f\left(x_1\right) = \begin{cases} x_1 - 1 & x_1 \geq 1\\ 0 & -1 \leq x_1 \leq 1\\ x_1 + 1 & x_1 \leq -1,\end{cases} \tag{21}$$

and the system can also be expressed as a uniform

$$\dot{X} = F^{(i)}\left(x, t, \mu_i\right), \quad i \in \{1, 2, 3\} \tag{22}$$

where $F^{(1)}(x,t,\mu_1) = (x_2, -2\xi x_2 - (1 + k_1\cos(\omega t))(x_1 - 1) + f_{av} + f_e\omega^2\cos(\omega t))^T$,
$F^{(2)}(x,t,\mu_2) = (x_2, -2\xi x_2 + f_{av} + f_e\cos(\omega t))^T$,
$F^{(3)}(x,t,\mu_3) = (x_2, -2\xi x_2 - (1 + k_1\cos(\omega t))(x_1 + 1) + f_{av} + f_e\omega^2\cos(\omega t))^T$.

μ_i, $i = 1 \sim 3$, represent system parameters. In order to obtain the sliding dynamics along the separation boundaries, the differential inclusion theory will be introduced.

For (22), it can also be expressed as

$$\dot{X} \in F(x, t, \lambda), \quad X = \left(X_1, X_2\right)^T \in D_i \cup D_j \cup D_{ij} \tag{23}$$

The set-valued vector field $F(X, t, \lambda)$ is convex and continuous with respect to the parameter λ contained in the closed interval $[0, 1]$. The following property holds for the convex set of the vector field.

$$F(x, t, \lambda) = \begin{cases} F^{\alpha}\left(x, t, \mu_\alpha\right) & \lambda = 0\\ F^{0}\left(x, t\right) & \exists\lambda \in (0, 1)\\ F^{\beta}\left(x, t, \mu_\beta\right) & \lambda = 1\end{cases} \tag{24}$$

$\alpha, \beta \in \{i, j\}$, $\alpha \neq \beta$, and $F^{\alpha}(x,t,\mu_\alpha)$ and $F^{\beta}(x,t,\mu_\beta)$ are the input and output vector fields, respectively. $F^0(x,t)$ is a vector field along the separation boundary.

From the convexity of the set-valued vector field, we have

$$F^{0}\left(x, t\right) = \lambda F^{\beta}\left(x, t, \mu_\beta\right) + (1 - \lambda)\, F^{\alpha}\left(x, t, \mu_\alpha\right) \tag{25}$$

The sliding motion is along the separation boundary, which indicates the vector field is along the boundary. So $n_{D_{ij}}^T F^0(x,t) = 0$ from which we have

$$\lambda = \frac{n_{D_{ij}}^T F^{\alpha}\left(x, t, \mu_\alpha\right)}{n_{D_{ij}}^T\left[F^{\alpha}\left(x, t, \mu_\alpha\right) - F^{\beta}\left(x, t, \mu_\beta\right)\right]} \tag{26}$$

For our system, the separation boundaries are $x_1 \pm 1 = 0$, so the normal vector of separation boundaries is $n_{D_{12}} = n_{D_{23}} = (1, 0)^T$; then we get

$$\begin{aligned} n_{D_{12}}^T F^{(1)}\left(x, t, \mu_1\right) &= n_{D_{12}}^T F^{(2)}\left(x, t, \mu_2\right) = x_2\\ n_{D_{23}}^T F^{(2)}\left(x, t, \mu_1\right) &= n_{D_{23}}^T F^{(3)}\left(x, t, \mu_3\right) = x_2\end{aligned} \tag{27}$$

From (26) and (27), we can obtain $\lambda \longrightarrow \infty$. However, from the convexity, the parameter $0 < \lambda < 1$ is required. Therefore, a perturbation parameter δ is introduced for a new separation boundary ($x_1 + \delta x_2 = \pm 1$) near the original boundaries $x_1 \pm 1 = 0$; then

$$n_{D_{12}} = n_{D_{23}} = (1, \delta)^T \tag{28}$$

$$\begin{aligned} n_{D_{12}}^T F^{(1)}\left(x, t, \mu_1\right) &\neq n_{D_{12}}^T F^{(2)}\left(x, t, \mu_2\right) = x_2\\ n_{D_{23}}^T F^{(2)}\left(x, t, \mu_1\right) &\neq n_{D_{23}}^T F^{(3)}\left(x, t, \mu_3\right) = x_2\end{aligned} \tag{29}$$

Finally, the vector field on the new separation boundaries can be determined as $F^{(0)}(x,t) = (x_2, -x_2/\delta)^T$, so the sliding dynamics along the separation boundaries can be investigated by

$$\begin{pmatrix}\dot{x}_1\\ \dot{x}_2\end{pmatrix} = \begin{pmatrix}0 & 1\\ 0 & -\dfrac{1}{\delta}\end{pmatrix}\begin{pmatrix}x_1\\ x_2\end{pmatrix} \tag{30}$$

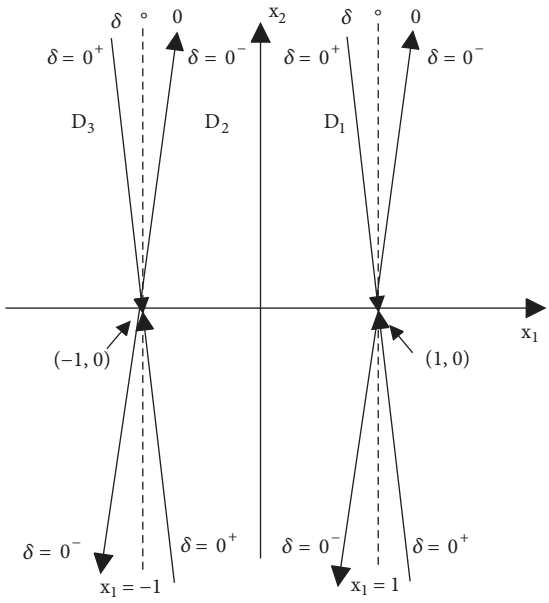

Figure 5: Sliding dynamics.

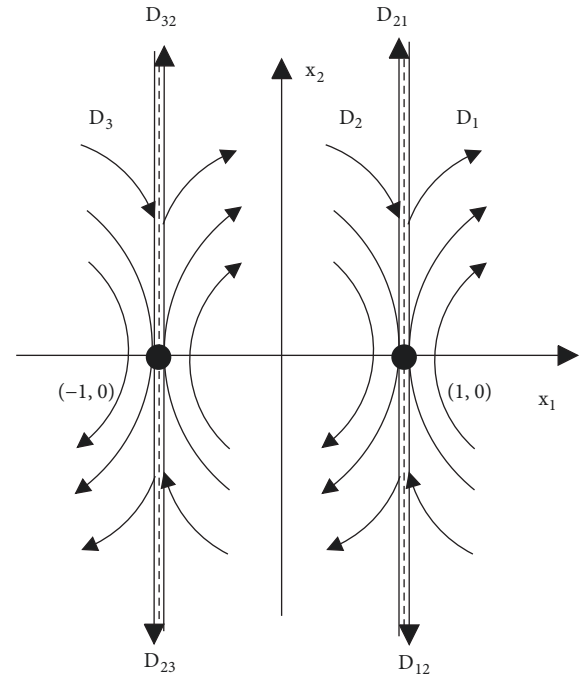

Figure 6: Topological structures of the flows.

With initial condition $(\pm 1, x_{20})$ at $t = 0$, the foregoing equation gives

$$x_1 = \pm 1 - \delta x_{20} e^{-t/\delta}, \quad x_2 = x_{20} e^{-t/\delta} \tag{31}$$

Since δ is very small, (31) can approximately describe the sliding dynamics along the separation boundaries. From (30), if $\delta \longrightarrow 0^+$, all the sliding motions on the two boundaries, respectively, approach the two static balance points (i.e., (±1, 0)) as $t \longrightarrow \infty$. However, for given $\delta \longrightarrow 0^-$, the sliding motions on the two boundaries, respectively, go away from the two static balance points. So the two balance points are like saddles as shown in Figure 5. But for $\delta \equiv 0$, the sliding dynamics along the separation boundaries $x_1 \pm 1 = 0$ are undetermined.

From the analytical conditions for grazing motions, the grazing bifurcation conditions on the separation boundaries for the flows of this nonsmooth system are

$$x_2 = 0, \quad \dot{x}_2 \neq 0 \quad \text{for } x_1 = \pm 1 \tag{32}$$

Therefore, in the neighborhoods of the two equilibrium points, the local topological structures can be sketched in Figure 6.

In order to verify the rationality of the topology, several grazing trajectories will be obtained. Herein, we make use of these grazing trajectories to approximately describe the sliding dynamics along the separation boundaries.

Choose the system parameters as $\xi = 0.024$, $k_1 = 0.06$, $\omega = 0.61$, $f_e = 0.25$, where f_{av} represents the constant forcing parameter and φ denotes the initial phase.

Consider the parameters $f_{av} = 0.075$, $\varphi = 4.47$, initial state (1,0.3); $f_{av} = 0.596$, $\varphi = 4.21$, initial state (1,0.4), respectively. Two grazing trajectories can be obtained as shown in Figure 7. The grazing points are both (1, 0). In the neighborhoods of (1, 0), the system trajectories conform to the topology above.

Suppose $f_{av} = 0.075$, $\varphi = 4.47$, initial state (1,0.3); $f_{av} = 0.596$, $\varphi = 4.21$, initial state (1,-0.3), respectively. We can also obtain two grazing trajectories in the points (-1, 0), (1, 0), respectively. As shown in Figure 8, they both conform to the topology above.

As shown in Figure 9, several grazing trajectories are obtained to draw on the same coordinates to approximately describe the sliding motions along the separation boundaries and to verify the topology in the neighborhood of grazing points.

4. Analysis of Periodic Response

For the gear transmission system, due to the existence of time-varying period stiffness and periodic excitation, the system must have periodic motion under certain system parameters' combination. Therefore, the external load is used as the conversion parameter, and the periodic response of the system is analyzed by the mapping method.

4.1. The First Case Periodic Motions. The system parameter adopts common parameter, which can be accessed from [2, 18]. Select the system parameters as follows: $\xi = 0.024$, $k_1 = 0.06$, $\omega = 0.61$, $f_e = 0.25$ $f_{av} = 0.25$. The system flow is always within the range $u \geq 1$ of intervals D_1 (Figure 2).

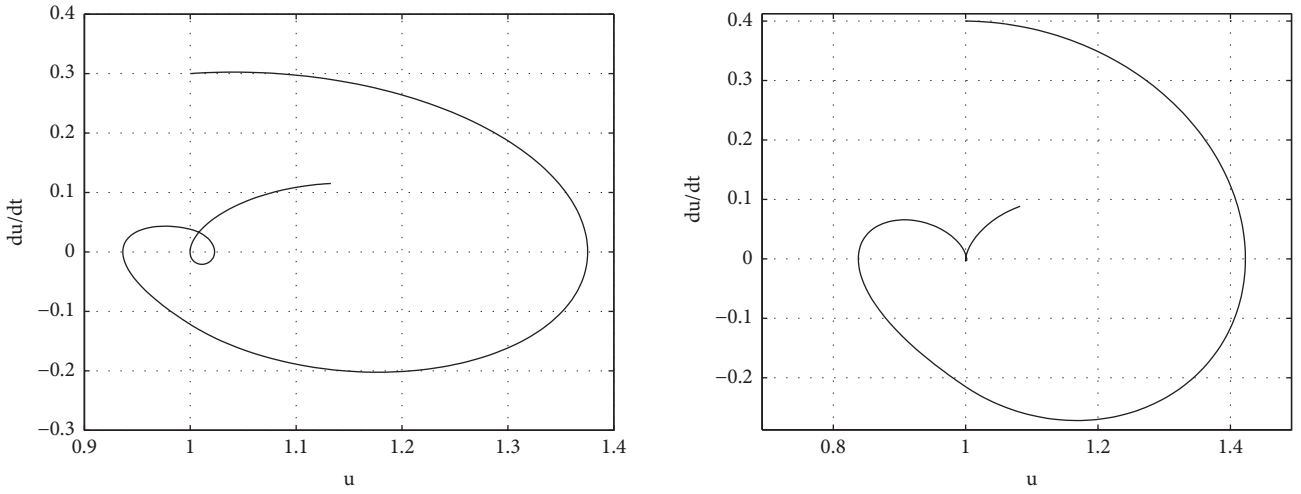

Figure 7: Grazing trajectories at (1,0).

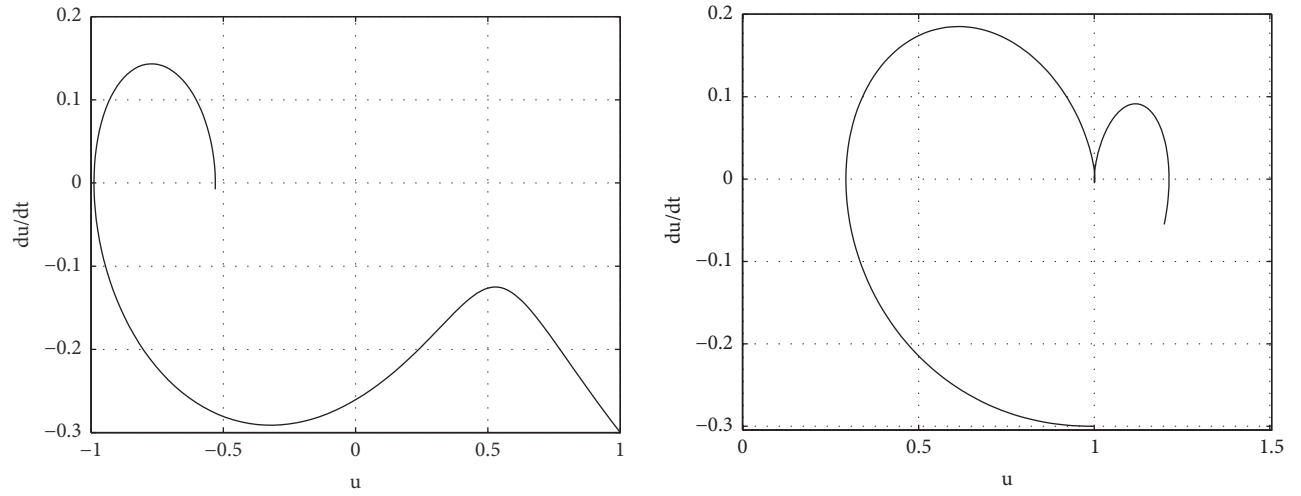

Figure 8: Grazing trajectories at (-1,0) and (1,0).

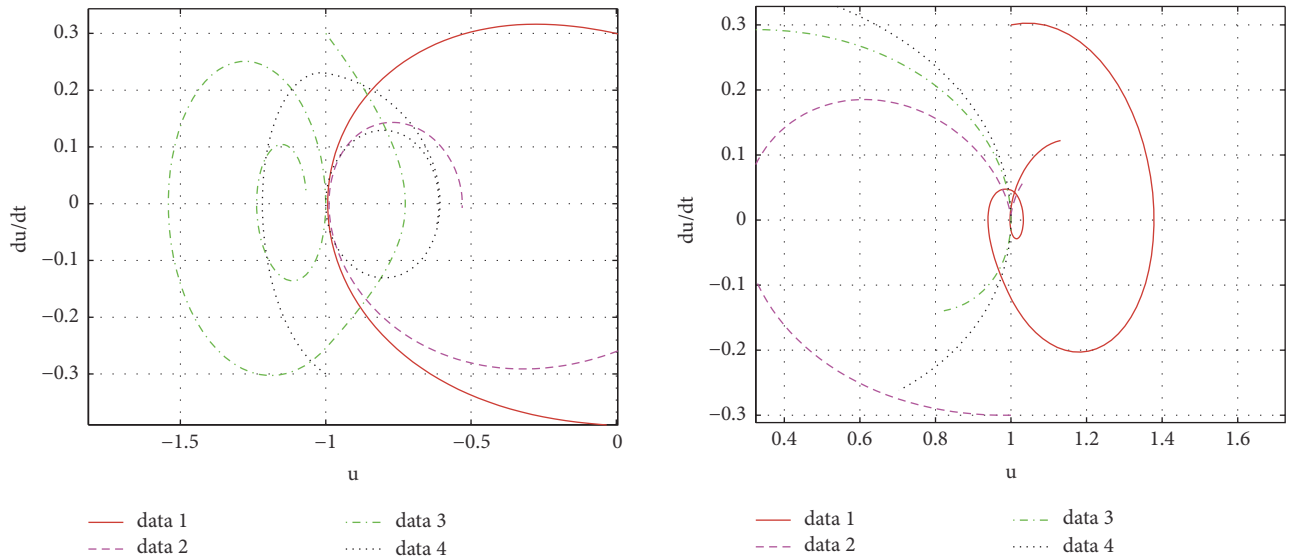

Figure 9: Combination of grazing trajectories.

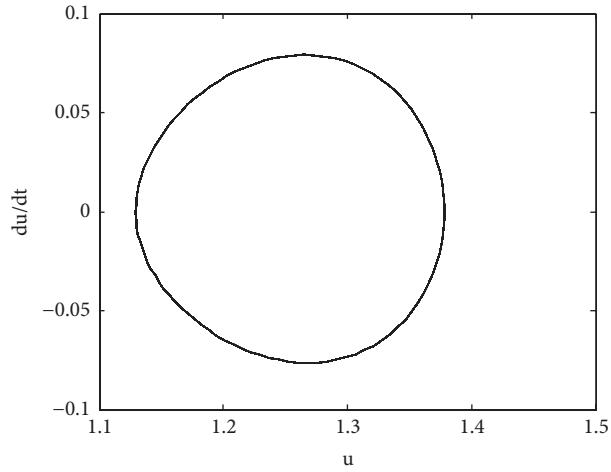

Figure 10: Phase diagram of meshing state.

The phase diagram is shown in Figure 10. The dynamics is constrained by the equation:

$$\ddot{u} + 2\xi\dot{u} + k(t)(u-1) = f_{av} + f_e\omega^2\cos(\omega t) \tag{33}$$

where $k(t) = 1 + k_1\cos(\omega t)$; $f_{av} = F_{av}/bk_0$; $f_e = e_m/b$.

4.2. The Second Case Periodic Motion. For the gear transmission system, the second case periodic motion that corresponds to the collision state of the gear can be divided into two cases: single-sided impact periodic motions and double-sided impact periodic motions.

4.2.1. Single-Sided Impact Periodic Motions. When $f_{av} = 0.223$, other parameters remain the same. In this case, the maximum value of the corresponding periodic flow is bigger than 1, the minimum value is between the two constraint surfaces $u = \pm 1$. The gear system operates in a single-sided impact periodic motions, and the teeth are transitioning between the two states of disengagement and engagement. The phase diagram is shown in Figure 11.

For the convenience of research, assuming the initial state of the periodic motion is a fixed point on the interface ∂D_{21}, as shown in Figure 12. At this point the system flow consists of two parts; one is in the interval D_1 and the other is in the interval D_2. For the trajectory in D_1, the dynamic is constrained by (33), and the corresponding basic mapping is P_1; for the trajectory in D_2, the dynamic is determined by (34), and the corresponding basic mapping is P_5.

$$\ddot{u} + 2\xi\dot{u} = f_{av} + f_e\omega^2\cos(\omega t) \tag{34}$$

In this case, the system flow moves through the constraint surface. In order to establish the periodic mapping corresponding to periodic motion, it is necessary to introduce discontinuous mappings S_{21} and S_{12} to compensate for the discontinuity of the system flow and then use the mapping compound rule to obtain the periodic mapping PT.

Suppose $x_1 = u$, $x_2 = \dot{u}$; then the system (7) can be expressed as follows:

In interval D_1,

$$f_{p+}: \begin{cases} \dot{x}_1 = x_2 \\ x_2 = -2\xi x_2 - \left(1 + k_1\cos(\omega t)\right) * \left(x_1 - 1\right) + f_{av} + f_e\omega^2\cos(\omega t) \end{cases} \tag{35}$$

In interval D_2,

$$f_{p-}: \begin{cases} \dot{x}_1 = x_2 \\ \dot{x}_2 = -2\xi x_2 + f_{av} + f_e\omega^2\cos(\omega t) \end{cases} \tag{36}$$

According to the noncritical discontinuous mapping,

$$S_{21} = I + \frac{\left(f_{p+} - f_{p-}\right)\nabla h}{\nabla h f_{p-}} = I \tag{37}$$

$$S_{12} = {S_{21}}^{-1} = I \tag{38}$$

Therefore, the periodic mapping is

$$PT = S_{21}\cdot P_5\cdot S_{12}\cdot P_1 = P_5\cdot P_1 \tag{39}$$

4.2.2. Double-Sided Impact Periodic Motions. When $f_{av} = 0.233$, other parameters remain the same. A steady periodic state can be obtained as shown in Figure 13. In this case, the maximum value is bigger than 1 and the minimum value is smaller than -1. This state corresponds to the double-sided impact.

As shown in Figure 14, the initial state still selects the fixed point on interface ∂D_{21}. Adopting the similar method above, the periodic mapping could be obtained as

$$PT = S_{12}\cdot P_4\cdot P_{23}\cdot P_3\cdot S_{32}\cdot P_2\cdot S_{21}\cdot P_1 \tag{40}$$

As $S_{12} = S_{21} = S_{23} = S_{32} = I$, then

$$PT = P_4\cdot P_3\cdot P_2\cdot P_1 \tag{41}$$

5. Stability Analysis

In this section, these mapping structures will be used to analyze the periodic motion stability of the system through Floquet theory. At the same time, in order to judge whether the system enters the chaotic state, the maximum Lyapunov exponent spectrum of the system is obtained. That paper takes the double-sided impact case as an example to demonstrate the mapping method of stability analysis. Its

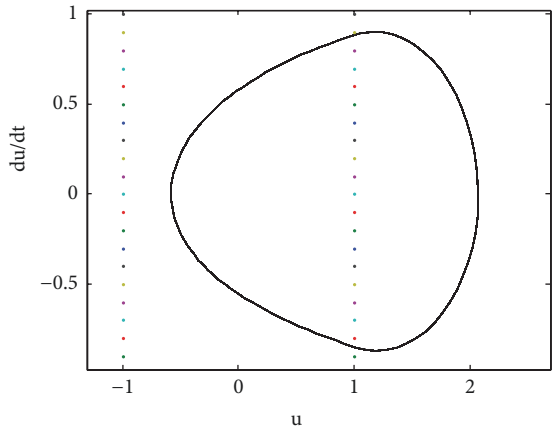

Figure 11: Single-sided impact.

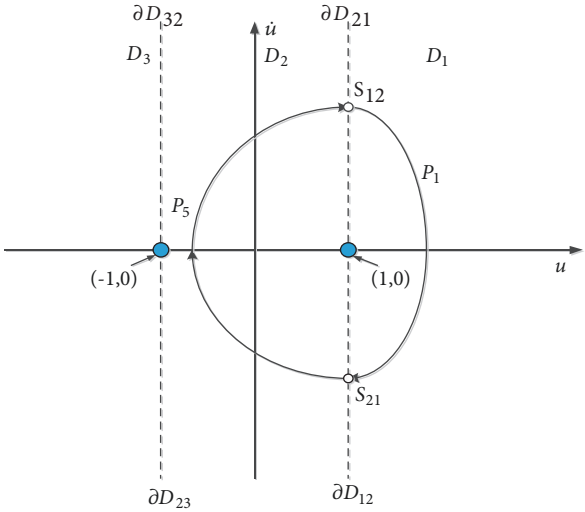

Figure 12: The mapping structures.

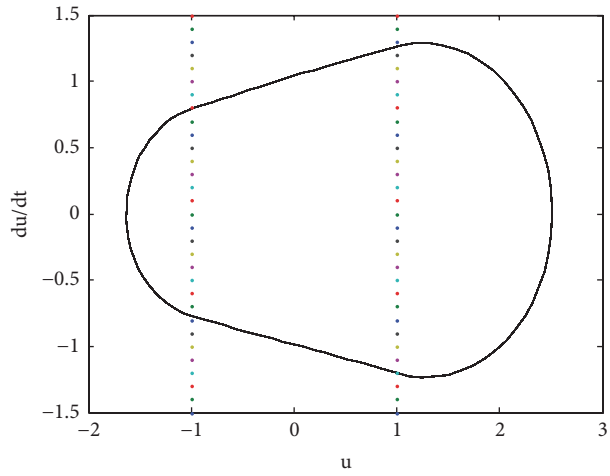

Figure 13: Double-sided impact.

corresponding periodic mapping is $PT = P_4 \cdot P_3 \cdot P_2 \cdot P_1$. The stability and bifurcation for periodic motion can also be confirmed through the periodic mapping PT which is corresponding to Jacobi matrix. By the chain rule, the Jacobi matrix can be expressed as follows:

$$DP = DP_4 \cdot DP_3 \cdot DP_2 \cdot DP_1 \tag{42}$$

For DP_i, $i = 1 \sim 4$, due to the time-varying stiffness of the gear system and backlash, DP_i has difficulty in getting the analytical form of its system flow, so the analysis of each mapping form can not be got. But they can be obtained through numerical method, such as the shooting method. At the same time, the corresponding Jacobi matrix can be yielded.

Suppose that the Jacobi matrix DP of periodic motion has been obtained, then the eigenvalues of a fixed point for this periodic mapping can be demonstrated as

$$\lambda_{1,2} = \frac{1}{2}\left[\mathrm{Tr}\,(DP) \pm \sqrt{\Delta}\right] \tag{43}$$

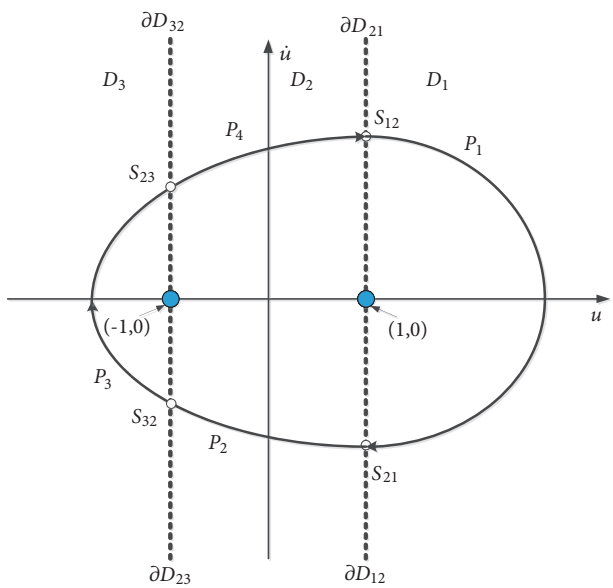

Figure 14: The mapping structure.

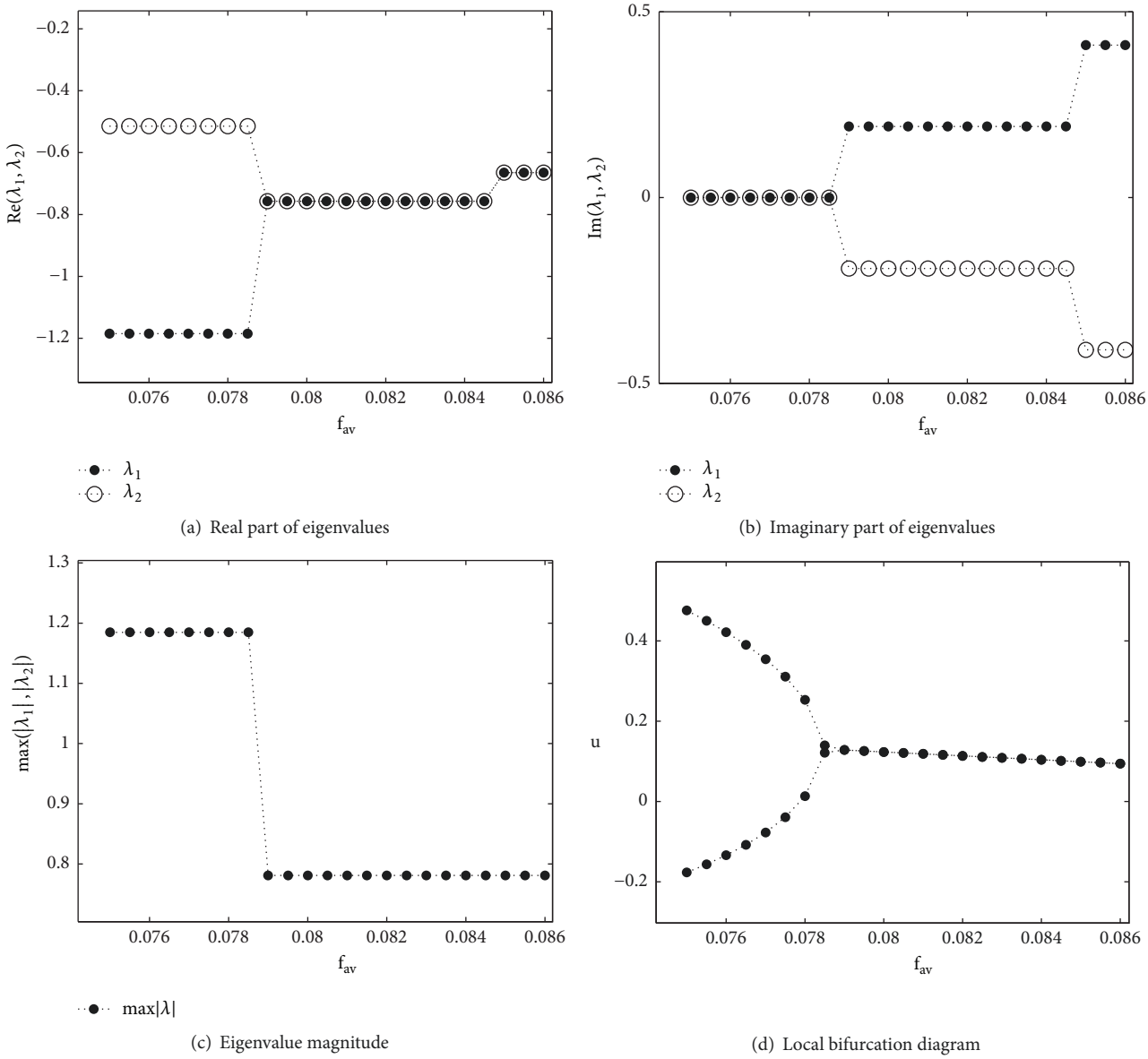

Figure 15: Floquet multiplier map and bifurcation diagram.

Tr(DP) represents the trace of DP; Det(DP) denotes the determinant of DP.

$\Delta = [\mathrm{Tr}(DP)]^2 - 4\mathrm{Det}(DP)$. If $\Delta < 0$, (43) can be demonstrated through

$$\lambda_{1,2} = \mathrm{Re}(\lambda) \pm j\mathrm{Im}(\lambda) \tag{44}$$

$j = \sqrt{-1}$; $\mathrm{Re}(\lambda) = (1/2)\mathrm{Tr}(DP)$; $\mathrm{Im}(\lambda) = (1/2)\sqrt{|\Delta|}$.

For $\lambda_{1,2}$, the period-1 motion will be stable if they are located in the unit circle. But if one of them is located outside the unit circle, then the period-1 motion will be unstable. This means that only if $|\lambda_{1,2}| < 1$, the periodic motion of the system is stable.

If one eigenvalue is -1 and the other is within the unit circle, the periodic doubling bifurcation is going to occur.

If one eigenvalue is +1 and the other is within the unit circle, the saddle-node bifurcation is going to occur.

Therefore, an improved shooting method is adopted to calculate the variation of the Floquet multiplier when the system changes with the external load parameters. The principle of the shooting method is to convert the two-point boundary value problem into the initial value problem. When the shooting method is used to calculate the Floquet multiplier, the Floquet multiplier is discrete and parameterized in the time domain. According to the change of Floquet multiplier, the stability of the system's periodic motion and the way of instability are predicted. The Floquet multiplier map and the corresponding bifurcation diagram in the interval [0.075,0.086] are also presented as shown in Figure 15.

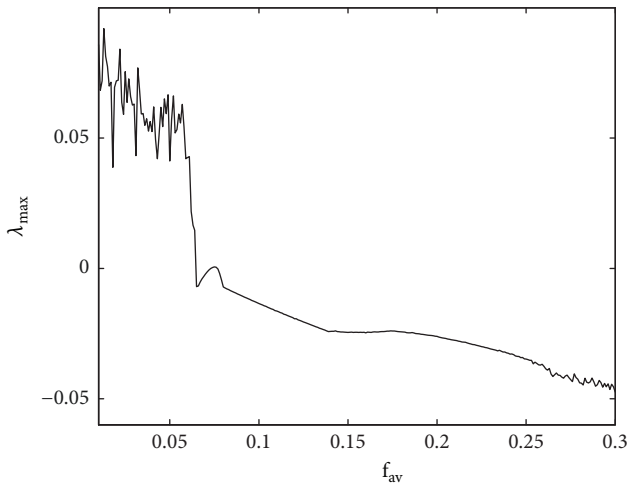

Figure 16: The maximum Lyapunov exponent spectrum.

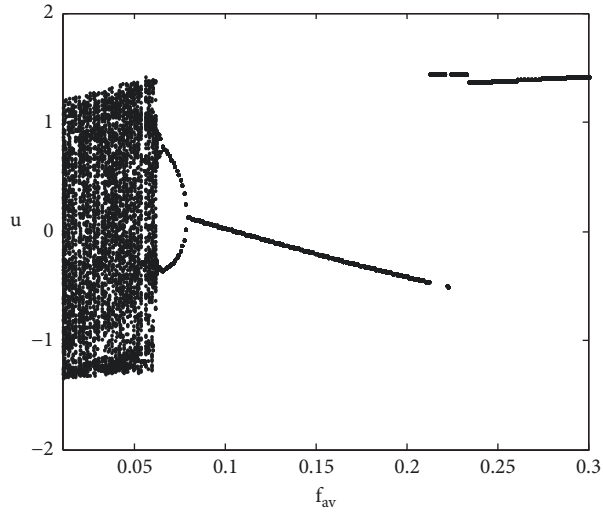

Figure 17: Bifurcation diagram.

From Figure 15, we can deduce that when $f_{av} \geq 0.079$ both eigenvalues are located in the unit circle, which implies that corresponding period-1 motion is stable. When f_{av} is at the vicinity of 0.0785, one of the two eigenvalues jump out the unit circle from -1. Meanwhile the other is still within the unit circle, which indicated the period doubling bifurcation takes place.

By using the Floquet theory, we can merely get the stability and bifurcation of periodic motions. For judging the chaos state, other effective methods need to be introduced. As the Lyapunov exponent spectrum is one of the most precise tools to determine the chaos state, therefore, the maximum Lyapunov exponent spectrum is presented in Figure 16.

From Figure 16, we can deduce that when $f_{av} \geq 0.06$, the maximum Lyapunov exponents are negative, which implies the system does not enter the chaos state. When $f_{av} \leq 0.06$, the maximum Lyapunov exponents are positive, which implies the system is under chaos state. By comparing the result with the bifurcation diagram and Poincare section, consistent conclusions can be obtained. For the sake of demonstrating this system and ensuring the conclusion above, the system bifurcation of the gear system with external load parameters f_{av} is shown in Figure 17. Enlarging the 0.06 - 0.08 part of bifurcation diagram, we can get the local bifurcation diagram as demonstrated in Figure 18.

The bifurcation diagram is used in the process of simulation. Bifurcation refers to small and continuous changes in the parameters of the system. As a result, the nature or topological structure of the system suddenly changes.

Poincare is a method for discretizing continuous systems and the Poincare map can replace the n order continuous system by using the discrete mapping of order $n - 1$. The Poincare map is used to reduce the order of the system, and the Poincare map builds a bridge between the continuous system and the discrete system.

In order to demonstrate the transition process in detail, suppose f_{av} =0.08, 0.078,0.064,0.0624,0.058, respectively; both the Poincare section and the corresponding phase diagram are gained as demonstrated in Figure 19.

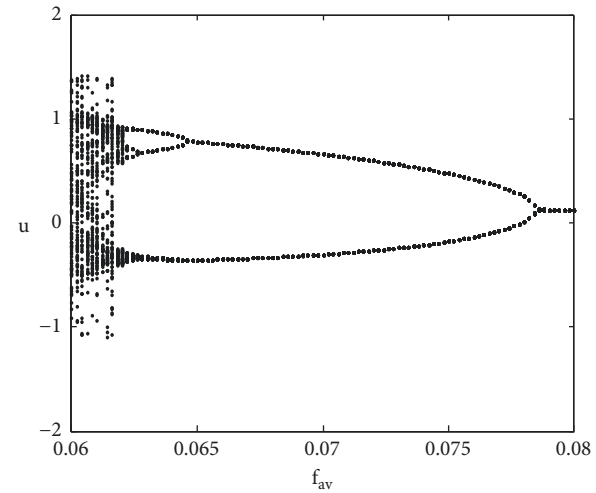

Figure 18: Local bifurcation diagram.

6. Conclusions

Firstly, for common gear systems, a nonlinear vibration model with backlash, time-varying stiffness, and static transmission error is established. The nonsmooth characteristics of the system are analyzed theoretically. According to the model, the state of motion is summarized into three main cases. For the period motion, the corresponding Poincare mapping is established. In order to analyze the stability of the periodic motion of the system, the discrete-time shooting method was adopted to calculate the variation of the Floquet multiplier. Then, the Floquet theory and the idea of mapping are used to give methods and conditions for judging the stability of the system's periodic response. At the same time, to judge the chaotic state of the system, the maximum Lyapunov exponent of the system is obtained. Finally, in order to verify the rationality of the above method, the global bifurcation diagram of the system is gained. Through the comparison, the same conclusion can be got, the whole process of the system

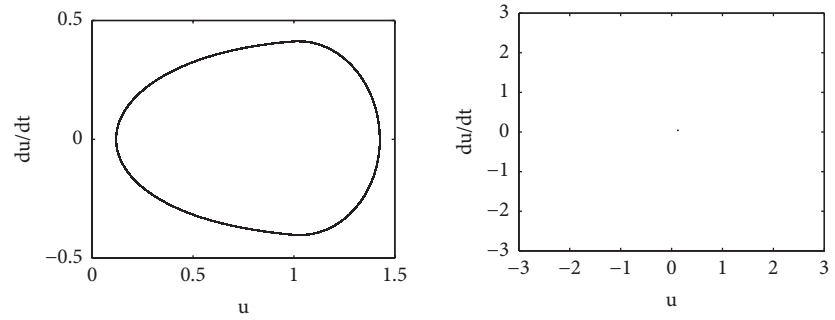

(a) $f_{av} = 0.08$

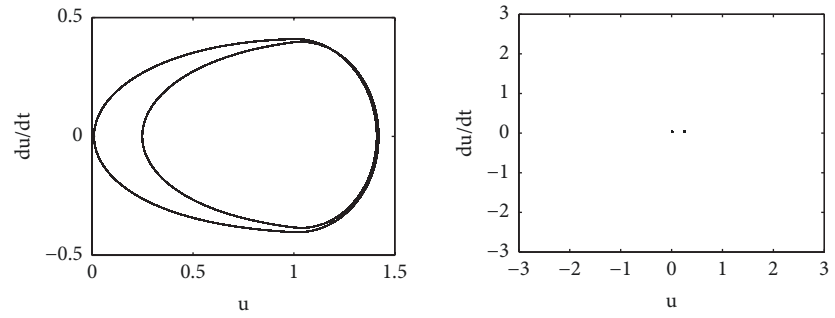

(b) $f_{av} = 0.078$

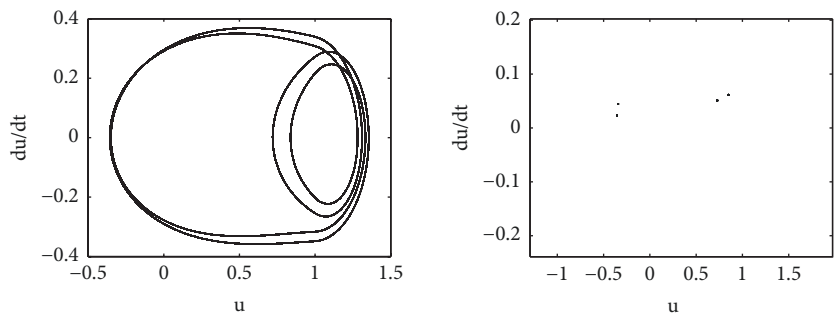

(c) $f_{av} = 0.064$

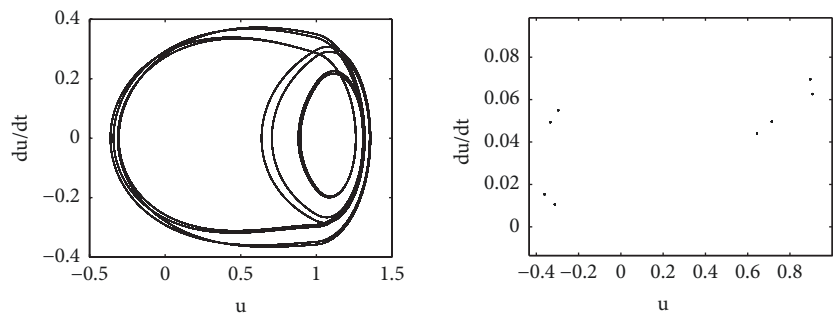

(d) $f_{av} = 0.0624$

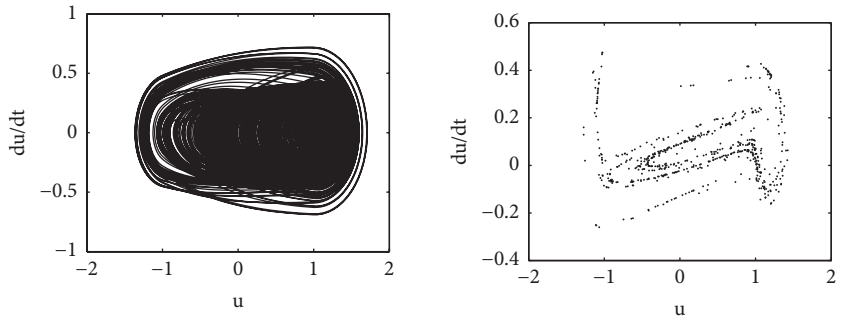

(e) $f_{av} = 0.058$

Figure 19: Phase diagrams and Poincare sections.

from the periodical bifurcation to the chaos is given, and a reasonable explanation for the jumping phenomenon in the bifurcation diagram is given.

Through the study of the gear system we can get the following conclusions. When the external load of the gear system is large, it is in a fully engaged state; as the load decreases, the state of motion changes from full meshing to unilateral collisions and bilateral collisions. In addition unilateral collisions and bilateral collisions occur alternately. As the load continues to decrease, the stable periodic motion of the system begins to lose its stability, and the motion state enters chaotic state through periodic bifurcation. This conclusion has important practical value, which can guide us in the actual project to select reasonable load parameters.

As a complex nonlinear system, the gear system not only includes backlash, time-varying stiffness, and static transmission error of these nonsmooth factors, but also includes many other nonsmooth factors. Therefore, how to improve the system's nonsmooth characteristics in the further is an important research direction. In addition, how to avoid chaos by taking effective measures is also a future research tendency.

Data Availability

The data used to support the findings of this study are available from the corresponding author upon request.

Conflicts of Interest

The authors declare that they have no conflicts of interest.

Acknowledgments

This work was supported by Proceedings of the 2017 International Conference on Advances in Construction Machinery and Vehicle Engineering, the China Postdoctoral Science Foundation funded project (Grant no. 2017M620096), and the Natural Science Foundation of Hebei Province, China (Grant no. E2017203144).

References

[1] S. Theodossiades and S. Natsiavas, "Non-linear dynamics of gear-pair systems with periodic stiffness and backlash," *Journal of Sound and Vibration*, vol. 229, no. 2, pp. 287–310, 2000.

[2] S. Wang, Y. Shen, and H. Dong, "Chaos and bifurcation analysis of a spur gear pair with combined friction and clearance," *Jixie Gongcheng Xuebao/Chinese Journal of Mechanical Engineering*, vol. 38, no. 9, pp. 8–11, 2002.

[3] X.-S. Wang, S.-J. Wu, X.-H. Zhou, and Q.-L. Li, "Bifurcation and chaos in a nonlinear dynamic model of spur gear with backlash," *Zhendong yu Chongji*, vol. 27, no. 1, pp. 53–56, 2008.

[4] Y. Shen, S. Yang, and X. Liu, "Nonlinear dynamics of a spur gear pair with time-varying stiffness and backlash based on incremental harmonic balance method," *International Journal of Mechanical Sciences*, vol. 48, no. 11, pp. 1256–1263, 2006.

[5] J.-Y. Tang, W.-T. Chen, S.-Y. Chen, and W. Zhou, "Wavelet-based vibration signal denoising with a new adaptive thresholding function," *Journal of Vibration and Shock*, vol. 28, no. 7, pp. 118–121, 2009 (Chinese).

[6] A. Kahraman and R. Singh, "Non-linear dynamics of a spur gear pair," *Journal of Sound and Vibration*, vol. 142, no. 1, pp. 49–75, 1990.

[7] G. W. Blankenship and A. Kahraman, "Steady state forced response of a mechanical oscillator with combined parametric excitation and clearance type non-linearity," *Journal of Sound and Vibration*, vol. 185, no. 5, pp. 743–765, 1995.

[8] A. Raghothama and S. Narayanan, "Bifurcation and chaos in geared rotor bearing system by incremental harmonic balance method," *Journal of Sound and Vibration*, vol. 226, no. 3, pp. 469–492, 1999.

[9] J. Wang, J. Zheng, and A. Yang, "An analytical study of bifurcation and chaos in a spur gear pair with sliding friction," *Procedia Engineering*, vol. 31, no. 1, pp. 563–570, 2012.

[10] A. Kahraman and R. Singh, "Nonlinear dynamic of geared rotor-bearing system with multiple clearances," *Journal of Sound and Vibration*, vol. 144, no. 3, pp. 469–506, 1991.

[11] C.-W. Chang-Jian, "Strong nonlinearity analysis for gear-bearing system under nonlinear suspension-bifurcation and chaos," *Nonlinear Analysis: Real World Applications*, vol. 11, no. 3, pp. 1760–1774, 2010.

[12] J. Hartog and S. Mikina, "Forced vibrations with non-linear spring constants," *Journal of Applied Mechanics*, vol. 58, pp. 157–164, 1932.

[13] S. W. Shaw and P. J. Holmes, "A periodically forced piecewise linear oscillator," *Journal of Sound and Vibration*, vol. 90, no. 1, pp. 129–155, 1983.

[14] M. Kleczka, E. Kreuzer, and W. Schiehlen, "Local and global stability of a piecewise linear oscillator," *Philosophical Transactions Physical Sciences & Engineering*, vol. 338, no. 1651, pp. 533–546, 1992.

[15] A. C. J. Luo, "Analytical modeling of bifurcations, chaos and multifractals in nonlinear dynamics," 1996.

[16] A. B. Nordmark, "Non-periodic motion caused by grazing incidence in an impact oscillator," *Journal of Sound & Vibration*, vol. 145, no. 2, pp. 279–297, 1991.

[17] B. Blazejczyk, "Dynamics of a two-degree-of-freedom cantilever beam with impacts," *Chaos Solitons & Fractals*, vol. 40, no. 4, pp. 1991–2006, 2009.

[18] G. W. Luo, X. H. Lv, and Y. Q. Shi, "Vibro-impact dynamics of a two-degree-of freedom periodically-forced system with a clearance: diversity and parameter matching of periodic-impact motions," *International Journal of Non-Linear Mechanics*, vol. 65, no. 4, pp. 173–195, 2014.